ANALYSIS OF SALT EFFECTS ON THE DEPLETION OF FRACTURED RESERVOIR BLOCKS

Alfredo Battistelli [+], Claudio Calore [*] and Karsten Pruess [#]

[+] Aquater S p A , Via Miralbello 53, 61047 S Lorenzo in Campo (PS), Italy
[*] Istituto Internazionale per le Ricerche Geotermiche - CNR, Piazza Solfermo 2, 56126 Pisa, Italy
[#] Earth Sciences Division. Lawrence Berkeley Laboratory. 1 Cyclotron Road, Berkeley, CA 94720, USA

Key **words:**

numerical simulation. boiling reservoirs. salt precipitation, porosity and permeability reduction.

Abstract

To simulate flow problems in which the transport of a variable salinity hrine occurs, the TOUGH2 code with an equation-of-state module able to handle three-component mixtures of water, sodium chloride, and a non-condensible gas has been used. This EOS module can describe liquid and gas phases, and includes precipitation and dissolution of solid salt. The reduction of **rock** porosity because of salt precipitation is also considered, as well as the related decrease of formation permeability. We have simulated fluid production from tight matrix blocks under conditions considered representative of vapor-dominated systems to examine some effects of permeability reduction and vapor pressure lowering due to salinity. Block depletion occurs by a "well on deliverability" placed in the fractures, and cases with different initial NaCl concentration and matrix permeability have been studied. We find that for initial NaCl mass fractions above threshold values, "sealing" of the block occurs and large amounts of fluid may not be recovered. As sealing occurs in the outermost grid element, the matrix block partitioning according to the MINC method has been varied to analyze discretization effects.

1. INTRODUCTION

The thermodynamic and transport properties of geothermal fluids are very important for determining the natural state of a geothermal system and its behaviour under exploitation. Such fluids usually consist of complex mixtures of water, non-condensible gases (NCG) and salts dissolved in the liquid phase. As water always represents the main mixture component, its thennophysical properties are customarily used to model geothermal reservoirs. In some cases the content of other components is such that they can alter the reservoir performance significantly.

For the compositional simulation approach required to study high-salinity natural systems that also contain non-condensible gases, an equation-of-state (EOS) module was developed for LBL's multipurpose TOUGH2 numerical simulator (Battistelli *et al.*, 1993).

Other codes are available to simulate the behaviour of multi-component systems. Andersen et al. (1992) presented a PVT model to be included in a reservoir simulator for H_2O-NaCl-CO_2 mixtures. The possible precipitation of solid salt was not accounted for. A three-component, three-phase EOS module implementing salt precipitation and associated penneability changes is available for the STAR reservoir simulator (Pritchett, 1993). Studies are underway to set **up** a water-sodium chloride EOS module for the TOUGH2 simulator for high temperatures and pressures: McKibbin and McNabb **(1993)** presented an accurate description of phase boundaries of H_2O-NaCl system up to 1075 °C and 1.6 kbar. An H_2O-NaCl EOS module for the TETRAD simulator has been used by Shook (in press) to study the effects of brine on the formation of a high temperature reservoir in vapor-dominated systems.

We have used the TOUGH2 code with the EOS developed by Battistelli *et al.* (1993) and the no-gas option to study some effects of permeability reduction and vapor pressure lowering (VPL) due to salinity in the depletion of tight matrix blocks, under conditions considered representative of vapor-dominated systems. With the matrix block partitioned into 15 elements, according to the MMC method (Pruess and Narasimhan, 1985), and an initial matrix permeability of the order of microdarcy, we find that for initial NaCl concentrations above threshold values, "sealing" of the block occurs. As sealing occurs in the outermost grid element, the block partitioning has been varied to verify its effect on the threshold value. A more detailed and complete analysis is still under way.

2. MODELING APPROACH

The TOUGH2 code implements the general MULKOM architecture for coupled inultiphase, multicomponent fluid and heat flows (Pruess, 1983, 1991a). This EOS module was developed to simulate flow problems in which the transport of a variable salinity brine and a NCG occurs. The multiphase system is assumed to be composed of three mass components: water. sodium chloride and CO_2, or some other NCG. Whereas water and the NCG components may be present only in the liquid and gas phases, the salt component may be present dissolved in the liquid phase or precipitated to form a solid salt phase. The solubility of NaCl in the gas phase is neglected.

The three mass components formulation employed was developed by enhancing an already existing EOS module for simulating the non-isothermal flow of saline water and air (Pruess, 1991b). The treatment of precipitatiom'dissolution of sodium chloride has been introduced using the method employed to treat siinilar phenomena occurring for water-silica mixtures (Verma and Pruess, 1988). The reduction of rock porosity because of salt precipitation is taken into account. as well as the related decrease of formation permeability, and are described below. The formulation of H_2O-CO_2 fluid mixture basically follows that described by O'Sullivan et al. (1985). The dependence of brine thermophysical properties on salt concentration has been included following an updated version of the thermophysical package developed by Aquater for a wellbore numerical simulator (Battistelli, 1991). All relevant thennophysical properties are evaluated using a subroutine by subroutine structure, so that the correlations employed at present can be easily modified. The dependence of brine enthalpy, density, viscosity and vapor pressure on salt concentration has been accounted for. as well as the effect on NCG solubility and heat of solution in the brine. Transport of the mass components occurs by advection in liquid and gas phases; binary diffusion in the gas phase for steam and the NCG is accounted for. Diffusive and dispersive processes in the liquid phase are not included in the present TOUGH2 code formulation. It is assumed that the three phases (gas, liquid, and solid) are in local chemical and thermal equilibrium. and that no chemical reactions take place other than interphase mass transfer.

In the integral finite differences formulation used by TOUGH?. the mass balance equations are written in the following general form (Pruess, 199 la):

$$\frac{d}{dt}\int_{V_n} M^{(k)}\, dV = \int_{\Gamma_n} \mathbf{F}^{(k)} \cdot \mathbf{n}\, d\Gamma + \int_{V_n} Q^{(k)}\, dV \qquad (1)$$

where k=1,2,3, indicates water, NaCl and NCG components, respectively. A complete description of the nomenclature used is given at the end of the paper The accumulation and mass flux terms for the NaCl component (k=2) are written as follows

$$M^{(2)} = \phi\, S_c\, \rho_c + \phi\, S_l\, \rho_l\, X_l^{(2)} \qquad (2)$$

$$\mathbf{F}^{(2)} = -k\,\frac{k_{rl}}{\mu_l}\,\rho_l\, X_l^{(2)}\,(\nabla P_l - \rho_l\, \mathbf{g}) \qquad (3)$$

where S_s is the "solid saturation", defined as the fraction of pore volume occupied by solid salt.

3. THERMODYNAMIC PACKAGE DESCRIPTION

The primary variables used for single phase conditions are total pressure of reference phase, P, salt mass fraction, $X^{(2)}$, NCG mass fraction, $X^{(3)}$, and temperature. T. If the solid salt is present, the second primary variable is switched to solid saturation S_s. In two-phase conditions the third primary variable is switched from NCG mass fraction to gas phase saturation S_g.

Mass balances of water, salt and NCG components, together with the heat balance, are set up and solved by TOUGH2 using the Newtown-Raphson iteration method. During the iteration process, the EOS module must be capable of recognizing the appearance and disappearance of phases, and of providing all thermophysical properties of phases present. pertaining to the last updated primary variables.

A description of the main tests performed to recognize the phase transitions and of the equations used to calculate phases properties is given below.

Liauid conditions

First the test for phase change to two-phase conditions is made checking if total pressure exceeds the boiling pressure of fluid mixture:

$$P \overset{?}{\geq} P_{boil}(T,\ X_l^{(2)},\ X_l^{(3)}) \tag{4}$$

The liquid phase boiling pressure is calculated according to:

$$P_{boil} = P_{b\,sat}(T,\ X_l^{(2)}) + P^{(3)}(T,\ X_l^{(2)},\ X_l^{(3)}) \tag{5}$$

If the test fails, a change to the two-phase state is made initializing the gas phase saturation to a small non zero quantity. The bubbling pressure of NCG, $P^{(3)}$, is calculated according to tlenry's law and accounting for the salting-out effect.

The solid salt phase appears if the salt mass fraction in the liquid phase exceeds the halite solubility, If.

$$X_l^{(2)} > X_{sol}^{(2)}(T) \tag{6}$$

precipitation starts and the second primary variable is switched from salt mass fraction $X^{(2)}$ to "solid saturation" S_s. (10 + S_s is then used as second primary variable: since it is larger than 1 it can be distinguished from mass fractions, which are always betweeii 0 and 1). When Eq. (6) indicates that precipitation is starting S_s is initialized to a sinall non zero value. Conversely, when solid phase is present. its disappearance is recognized simply by $S_s < 0$. In this case the second primary variable is switched back to $X^{(2)}$, and is initialized with a value slightly smaller than the equilibrium solubility $X_{sol}^{(2)}(T)$.

The thermophysical properties of the liquid phase are calculated as follows. The density and viscosity are assumed to be the same as those for brine, with the assumption that the effect of dissolved gas can be neglected because of low gas solubility. Liquid phase density. viscosity and enthalpy are given by:

$$\rho_l = \rho_b(P,\ T,\ X_l^{(2)}) \tag{7}$$

$$\mu_l = \mu_b(P,\ T,\ X_l^{(2)}) \tag{8}$$

$$H_l = (1 - X_l^{(3)})\ H_b(P,\ T,\ X_l^{(2)}) + X_l^{(3)}\ H_l^{(3)}(P^{(3)},\ T) \tag{9}$$

Gas conditions

In single-phase gas conditions the salt component can he present only as solid precipitate, having neglected its (very small) solubility in the gas phase. The appearance of the liquid phase is tested checking the partial pressure of steam. $P^{(1)}$, against the vapor brine pressure:

$$P^{(1)} \overset{?}{<} P_{b\,sat}(T,\ X_{eq}^{(2)}) \tag{10}$$

The hrine vapor pressure is calculated assuming $X_{eq}^{(2)} = 0$ if no solid phase is present in the element. otherwise the solubility of NaCI at element temperature is used. Partial pressure of water component is calculated using an iterative procedure froin total pressure. temperature and NCG mass fraction.

If the above test fails. a transition to two-phase conditions is diagnosed. initializing the third variable as a gas phase saturation slightly lower than one.

Density, enthalpy and viscosity of single-phase gas fluid mixtures are calculated as follows:

$$\rho_g = \rho_g^{(1)}(P^{(1)},\ T) + \rho_g^{(3)}(P^{(3)},\ T) \tag{11}$$

$$H_g = (1 - X_g^{(3)})\ H_g^{(1)}(P^{(1)},\ T) + X_g^{(3)}\ H_g^{(3)}(P^{(3)},\ T) \tag{12}$$

$$\mu_g = (1 - X_g^{(3)})\ \mu_g^{(1)}(P^{(1)},\ T) + X_g^{(3)}\ \mu_g^{(3)}(P^{(3)},\ T) \tag{13}$$

Liquid-gas mixtures

For elements with two-phase fluid the phase transition tect is made checking the gas phase saturation that is used as third primary variable. If $S_g \geq 1 - S_s$. then the liquid phase disappears and a transition to single-phase gas conditions is made. If $S_g \leq 0$. then the gas phase disappears and a transition to single-phase liquid conditions is made. Appearance or disappearance of a precipitated solid phase is handled as in liquid conditions.

With the assumption of additivity of partial pressures, the partial pressure of NCG is given by:

$$P^{(3)} = P - P_{b\,sat}(T,\ X_l^{(2)}) \tag{14}$$

The mole fraction of NCG in the liquid phase is calculated according to Henry's law:

$$Y_l^{(3)} = P^{(3)} / K_{hb}(T,\ m) \tag{15}$$

where m is the salt molality. Then thc inass fraction of NCG in the liquid phase is calculated in an obvious way. The mass fraction of NCG in the gas phase is calculated from the density of fluid mixture. computed considering an ideal mixture of steam and gas:

$$\rho_g = \rho_g^{(1)}(P_{b\,sat},\ T) + \rho_g^{(3)}(P^{(3)},\ T) \tag{16}$$

then:

$$X_g^{(3)} = \rho_g^{(3)} / \rho_g \tag{17}$$

The specific enthalpy and viscosity of vapor phase are calculated using Eq. 12 and 13 respectively. with $P^{(1)} = P_{b\,sat}$.

The density. viscosity and enthalpy of liquid phase are calculated with Eq. 7. 8 and 9 respectively. using the component inass fractions in the liquid phase.

4. MODELING OF PERMEABILITY REDUCTION

Changes in forination permeability due to precipitation or dissolution of halite are modeled using the porosity-permeability correlations given in the paper by Verma and Pruess (1988). They considered idealized models of permeable media to correlate the relative changes in permeability to the relative changes in porosity caused by the redistribution of a mineral in the pore space. The medium is assumed to have a set of non intersecting flow channels with either circular tubular or planar cross sections as shown in Figure 1.

As cross sections of actual flow channcls are highly variable. it can be expected that minor changes in average porosity may cause drastic permeability changes due to the closure of the narrow portions of pore throats. The "series models" shown in Figures 1c and Id are able to represent, even if in a rough way. the presence of "bottle-necks" in the flow channels. Because of this feature the permeability of porous medium can reduce to zero at a finite porosity ϕ_c . indicated as "critical porosity".

We summarize here below the equations corresponding to the tubular "series" model used for the simulations presented in this paper. The present EOS module implements all the permeability-porosity relationships corresponding to the pore models shown in Figure 1.

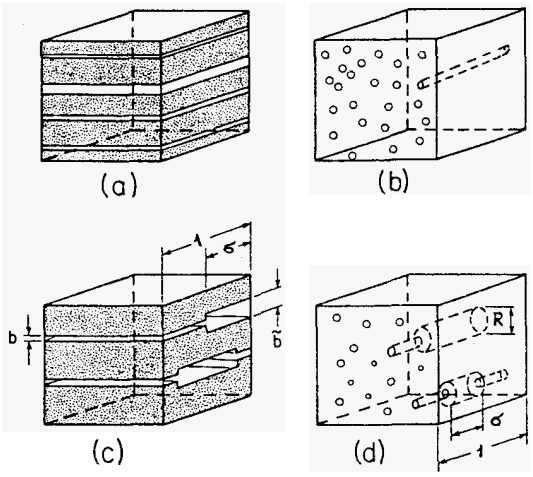

Figure 1. Idealized models of permeable media. Figures 1a and 1b represent the straight capillaric models, and figures 1c and 1d are the series models (after Verma and Pruess, 1988).

Assuming all tubes are identical and rate of deposition to be uniform, and considering the case of a single tube per unit area, initial porosity and permeability are given by:

$$\phi_o = \pi [\sigma R^2 + (1-\sigma) r^2] \tag{18}$$

$$\frac{1}{k_o} = \frac{8}{\pi}\left(\frac{\sigma}{R^4} + \frac{1-\sigma}{r^4}\right) \tag{19}$$

where R and r are tube radii and σ is the fractional length of tube with radius R. The critical porosity is equal to:

$$\phi_c = \phi_o - \pi r^2 \tag{20}$$

and the ratio of cross sectional areas is:

$$\Omega = (R/r)^2 \tag{21}$$

Introducing the normalized porosity:

$$\Theta = \frac{\phi - \phi_c}{\phi_o - \phi_c} \tag{22}$$

the porosity-permeability correlations for the tubular "series" model take the following form:

$$\frac{k}{k_o} = \Theta^2 \frac{1-\sigma+\sigma/\Omega^2}{1-\sigma+\sigma[\Theta/(\Theta+\Omega-1)]^2} \tag{23}$$

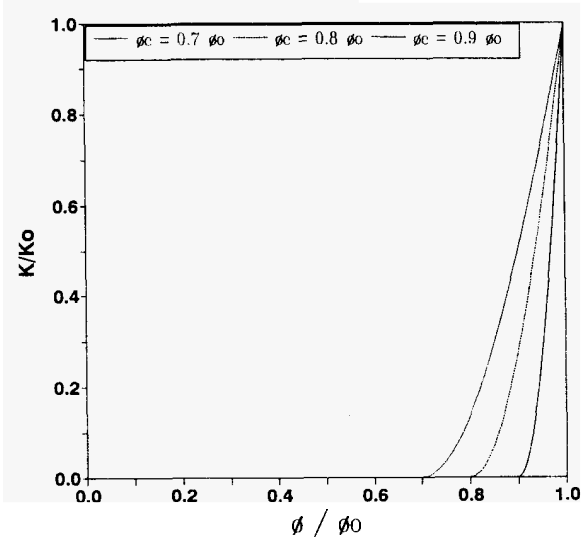

Figure 2. Permeability reduction factors for tubular series model and different critical porosity values.

Figure 2 shows the effect of critical porosity on permeability reduction factor for a fractional length of 0.8. It can be pointed out that a critical porosity equal to 80% of initial porosity means that the narrow pore throats are completely clogged when the solid saturation is 0.2 .

5. DEPLETION OF TIGHT MATRIX BLOCKS

Most of the fluid reserves in Lapor-dominated reservoirs are stored in tight matrix blocks with permeability of the order of microdarcy, and the fracture system is believed to contribute little to fluid storage, mainly providing large-scale permeability. We have, therefore, simulated fluid production from tight matrix blocks under conditions considered representative of vapor-dominated system to show some effects of permeability reduction and VPL due to salinity.

The model we used in our simulations consists of a single block of rock matrix in the shape of a cube with side length of 50 m, which is to be viewed as a subdomain of a large reservoir volume. The block is surrounded by fractures with a small fractional volume of 10^{-4}. The matrix block is discretized according to the MINC method (Pruess and Narasimhan, 1985) with 15 nested cubes of 0.5%, 1%, 2%, 3%, 4%, 5%, 6%, 7%, 8%, 9%, 10%, 10%, 11%, 11%, and 12.5% volume fractions. Matrix permeability, porosity density, specific heat and thermal conductivity are 5×10^{-18} m^2, 5%, 2600 kg/m^3, 920 J/kg °C and 2.51 W m °C, respectively. The system is initially in two-phase conditions at temperature of 240°C, with liquid saturation of 80% in the matrix block, and 1% in the fractures. Liquid relative permeability and capillary pressure are taken in the van Genuchten form, as used by Pruess and O'Sullivan (1992). Gas relative permeability is given by $k_{rg} = 1-k_{rl}$. Block depletion occurs by a "well on deliverability" placed in the fractures with prescribed wellbore pressure, P_{wb}, and productivity index, PI. Production rate in phase ß is then calculated as (Thomas, 1982):

$$q_\beta = \frac{k_{r\beta}}{\mu_\beta} \rho_\beta PI (P_\beta - P_{wb}) \tag{24}$$

Values of P_{wb} =1 MPa and PI = 1.788×10^{-13} m^3 have been used in our simulations. We modelled the permeability reduction using the series model for tubular flow with fractional length = 0.8 and $\phi_c/\phi_o = 0.8$.

Six cases are considered with different initial salt content. The effects of salt content on initial pressure and fluid reserves are shown in Table 1.

Table 1. Initial total pressure and fluid reserves for different salt contents.

Case	Salinity (% by weight)	Pressure (MPa)	Mass in place (Mkg)	Water in place (Mkg)
1	0	3.348	4.089	4.089
2	5	3.244	4.306	4.092
3	8	3.175	4.435	4.082
4	8.5	3.163	4.457	4.080
5	15	2.989	4.736	4.028
6	20	2.839	4.948	3.962

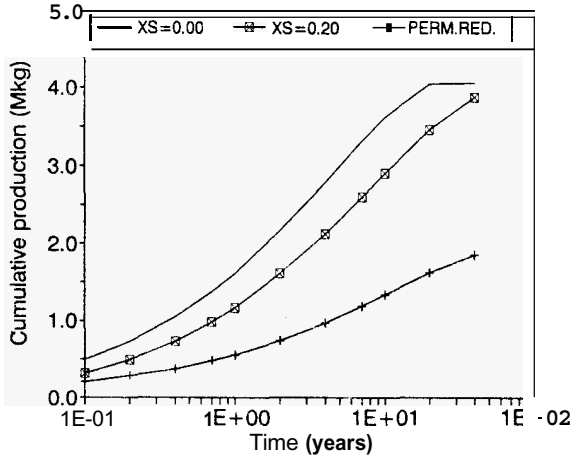

Figure 3. Effects of VPL and permeability reduction on cumulative fluid recovery

Figure 3 shows the cumulative production vs time for cases 1 and 6. Case 6 has been run with and without the permeability reduction to separate the effects of VPL and permeability reduction due to salt precipitation. Producing by a well on deliverability, the lower cumulative production for Case 6 without permeability reduction is due to the lower initial reservoir pressure. For case 1 the system is depleted after about 20 years, when all the matrix elements are in single-phase gas conditions. The same occurs for case 6 after about 40 years. with cumulative production almost equal to case 1. This is because the initial reserves of water are almost equal for the two cases, and the salt dissolved into the liquid phase is not recovered since the well produces steam from the beginning of exploitation. The introduction of permeability reduction in case *6* is responsible for a much lower cumulative production: after 40 years, cumulative production is about 50% that of case 1.

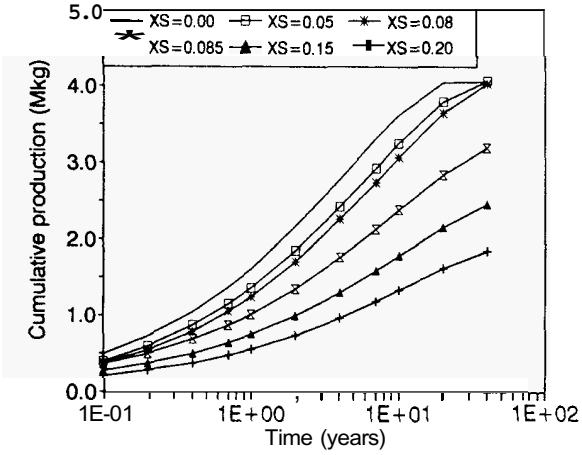

Figure 4. Cumulative fluid recovery for cases 1 to *6*

The effects of permeability reduction as a function of initial salt content are presented in Figure 4, which shows the cumulative mass production vs time for the six cases. It is interesting to note that when initial salt mass fraction is increased from *0.08* to *0.085,* the production history changes drastically, starting from about 0.4 years. For the cases with a low initial salt content (<8.5%), the depletion behavior is similar to that shown in figure 3 for case **6** without permeability reduction.

The change in behavior is highlighted in Figures *5,* 6 and 7, which show the pressure, liquid phase saturation and salt inass fraction distribution in the matrix block after 0.4 and 10 years for cases 1, 2 and 6. At early times a high pressure decrease near the block surface develops due to the low matrix permeability, producing a strong vaporization. From the beginning, no liquid phase is produced towards the fracture because the liquid phase is held back by capillary forces. The salt thus accumulates in the first matrix element because of vaporization of brine, flowing towards the block surface from the interior, until salt precipitation takes place.

For an initial salt content lower than the threshold value, the first matrix element vaporizes completely, and the precipitation of solid salt is transferred to the second matrix element. Then, progressively, all the elements dry out with precipitation of solid salt occurring in each (Figures 6 and 7).

For an initial salt content higher than the threshold value, the accumulation of salt in the first element is so fast that its drying out is avoided. The reduction in permeability reduces the extracted mass rate and slows down the depletion associated processes. In these conditions all the matrix elements remain in two-phase conditions, as shown in Figure 6.

Thus *two* processes mainly control depletion behavior: the vaporization of the liquid phase, with the complete drying out of matrix elements, and the permeability reduction due to solid salt precipitation. The change between the two observed behaviors depends on which process prevails: at low salt content the first matrix element dries out before salt precipitation seals the matrix block surface.

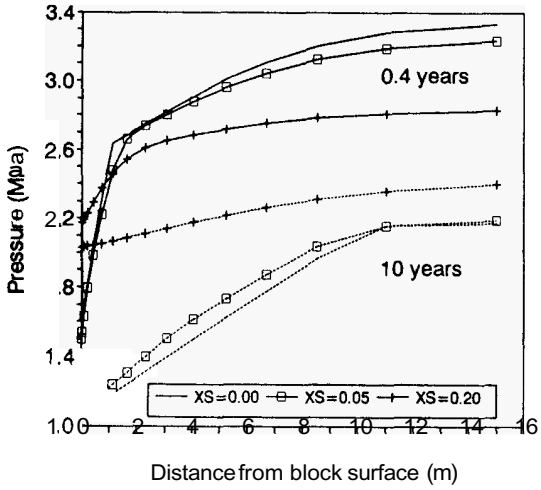

Figure 5. Pressure distribution vs distance from block surface after 0.4 and 10 years.

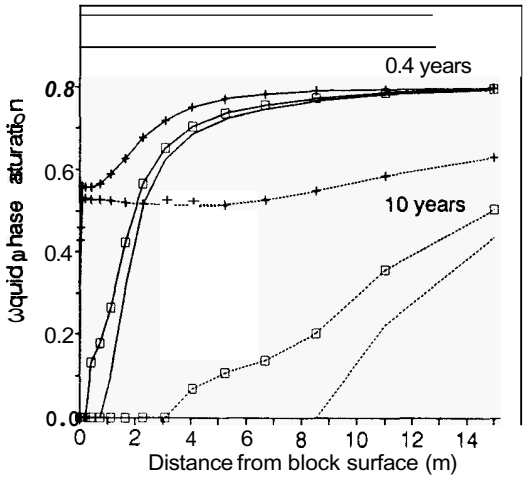

Figure 6. Liquid phase saturation distribution vs distance from block surface after 0.4 and 10 years.

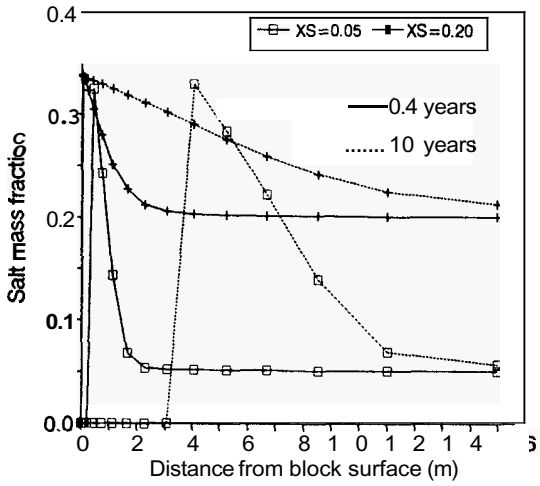

Figure 7. Salt mass fraction distribution vs distance from block surface after 0.4 and 10 years.

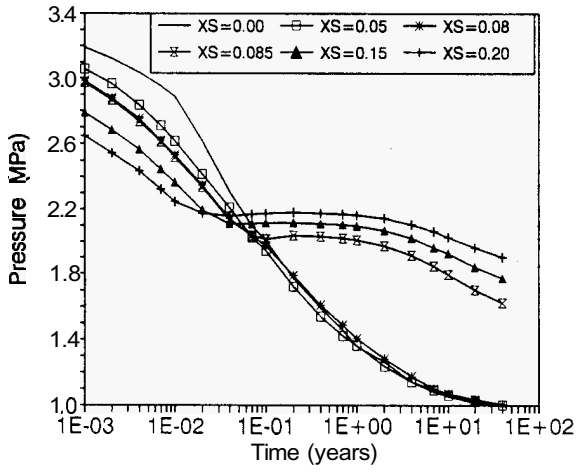

Figure 8. Pressure history in the first matrix element for cases 1 to 6

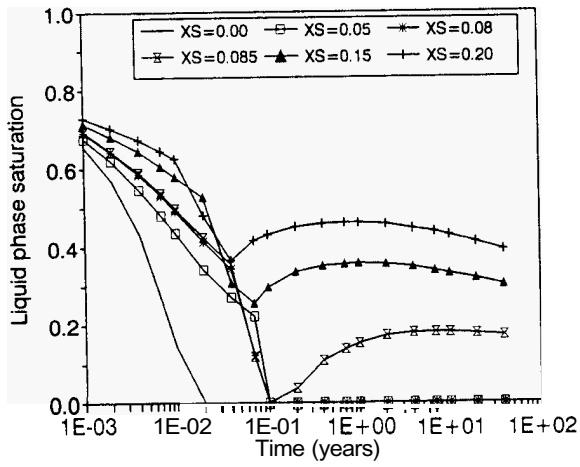

Figure 9. Liquid phase saturation history in the first matrix element for cases 1 to 6.

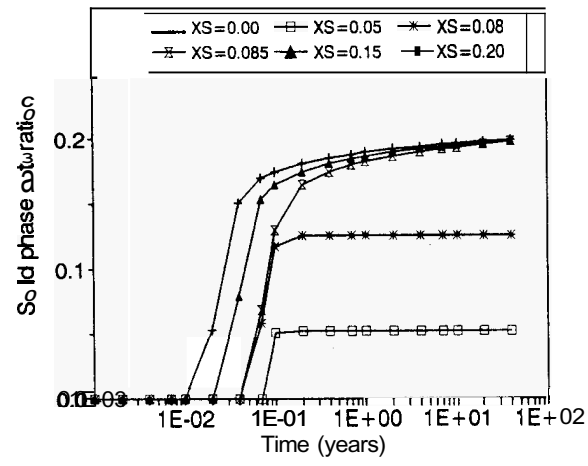

Figure 10. Solid phase saturation vs time in the first matrix element for cases 1 to 6.

To better show how these processes work, the pressure, liquid phase and solid phase saturations in the first matrix element are plotted as a function of time for all the six cases (Figures 8, 9 and 10).

At early time the liquid saturation decreases faster for lower initial salt content because of higher extraction rate. For higher initial salt content the deposition of solid salt starts earlier and reduces the rate of pressure depletion. If solid saturation approaches 0.20 before the drying out of the element, production is strongly reduced and consequently the pressure becomes almost stable in the element for up to about one year (Figure 8).

The increase in liquid saturation shown in Figure 9 for salt contents above the threshold value corresponds to the stabilization of pressure and is due to the equilibration of pressure inside the block. The same figure shows that the behaviors of Case 3 and 4 are practically the same until the liquid phase disappears after 0.1 years. Then. for a salt fraction of 0.085, i. e. slightly above the threshold value, the liquid phase appears again, due to the equilibration of pressure.

Below the threshold value the increase of solid saturation stops when the front of complete vaporization moves inside the block, and the liquid phase no longer vaporizes inside the first element (Figure 10). On the other hand. above the threshold value, the solid saturation asymptotically approaches 0.2, which is the value at which permeability becomes zero.

The change in behavior depends on events in the first matrix element. Since. at early times. a vaporization front is practically present close to the block surface, most boiling occurs in the first matrix element. In order to reduce to zero the permeability of the first element we need a fixed amount of salt. equal to:

$$M_{salt} = V_{element}\,(\phi_o - \phi_c)\rho_s \qquad (25)$$

For the present model this value, independent of initial salt content. is 13,500 kg. When initial salt content is low. a very large amount of brine has to vaporize to precipitate this amount of solid salt. In these conditions water vaporization prevails: the first element dries out, the front of complete vaporization moves inwards. and the block is completely depleted. When initial salt content is high, the same amount of precipitate is obtained with a much lower amount of vaporized brine: thus the second process prevails and block depletion is prevented by sealing of the block surface.

The results also indicate the possible effect of lower penneability and of a different grid discretization close to the block surface. With lower matrix permeahility. the depletion of the first matrix element will be faster because of a lower recharge from the interior of the block, and the threshold value will increase.

Using a finer discretization, by decreasing the volume of the first matrix eleinent. the amount of salt necessary to reduce permeability to zero will decrease. and the threshold value will also decrease.

The effect of a lower matrix penneability has been verified by running a second series of cases using a value of 10^{-18} m^2. In this case the recovery of fluid reserves is much slower and no complete depletion is achieved. even for the case of pure water case after 40 years. The change in behavior occurs for an initial salt fraction of about 0.095. The distributions of pressure, liquid saturation and salt mass fraction have a shape similar to the corresponding cases with a permeability of 5×10^{-18} m^2, but comparable values are reached at later times because of slower fluid production.

The effects of grid discretization have been checked by using block discretization5 with 10 and *30* elements, and fractional volumes of 0.02and 0.001. respectively, for the first matrix element. The change between the two characteristic behaviors occurs for initial salt mass fractions of 0.10-0.102. and 0.07-0.071, respectively. For initial salt contents outside the range of variation of the threshold value, block depletion behavior does not show large differences.

6. CONCLUSIONS

For the compositional simulation approach required to study high salinity natural systems that also contain non-condensible gases. a thennophysical properties package. developed for the wellbore flow code "PROFILI", was incorporated into the general-purpose multiphase tluid and heat flow code TOUGH2. Our formulation includes a comprehensive suite of multiphase mixture effects, including density. viscosity, and enthalpy effects from salt dissolution, reduction in non-condensible gas solubility due to salinity, vapor pressure lowering due to salinity, and porosity and permeability reduction from the precipitation of salt.

This simulator proved a valuable tool for improving our knowledge of

processes occurring in fractured reservoirs containing a brine. Numerical simulations have demonstrated that vapor pressure lowering effects from salinity are strong, and are likely to have a strong impact on the depletion of vapor-dominated systems. In the depletion of fractured reservoirs with low matrix permeability. persistent boiling near the surfaces of matrix blocks will lead to concentration and, ultimately, precipitation of solids. This may cause a severe loss in permeability. and may considerably slow the rates at which fluid reserves can be recovered. We find that for initial matrix permeability of the order of microdarcy, and NaCl concentrations above threshold values. "sealing" of the matrix block occurs. As sealing occurs in the outermost grid element. block partitioning according to the MINC method plays a crucial role.

ACKNOWLEDGEMENTS

This work was supported by Aquater S.p.A. of the Italian National Hydrocarbons Agency (ENI), by the International Institute tor Geothermal Research of the Italian National Research Council (CNR), and by the Assistant Secretary for Conservation and Renewable Energy, Geothermal Division, of the U.S. Department of Energy under contract No. DE-AC03-76SF00098.

Nomenclature

$\mathbf{F}^{(i)}$	mass flux of component i, kg (s m^2)
	acceleration of gravity. m^2/s
k	intrinsic permeability, m^2
K_h	Henry constant, Pa
k_r	relative permeability, dimensionless
m	salt molality, mol/kg
$M^{(i)}$	accumulation term of component i, kg/m^3
n	unit normal vector
P	pressure, Pa
PI	productivity index, m^3
q	production rate kg/s
$Q^{(i)}$	source term for component i. kg/(s m^3)
S	saturation
T	temperature, °C
V_n	volume of grid element n, m^3
$X^{(i)}$	mass fraction of component i
$Y^{(3)}$	mole fraction of NCG
$W^{(3)}$	molecular weight of NCG, kg/mol
ß	phase index (ß = liquid. gas)
A_n	surface area of grid element n, m^2
Θ	normalized porosity
μ	dynamic viscosity, Pa s
ρ	density, kg m^3
σ	fractional length
ϕ	porosity
Ω	area ratio for tube. equal to (R/r)^2

Subscripts and Superscripts

h	brine
boil	boiling
ß	phase
c	critical
eq	equivalent salt mass fraction
e	gas phase
l	liquid phase
s	solid salt phase
sat	vapor-saturated
sol	halite solubility
wb	wellbore
1	water component, H_2O
2	salt component NaCl
3	gas component, NCG

REFERENCES

Andersen, G., Probst. A., Murray. L. and Butler. S. (1992). An accurate PVT model for geothermal fluids as represented by H_2O-NaCl-CO_2 mixtures. *Proc 17th Workshop on Geoth Res. Eng.*, Stanford University, Stanford. pp. 239-248.

Battistelli, A. (1991). *PROFILI code: the thermodynamical package for H_2O NaCl-CO_2 fluid mixtures.* Aquater Report H 6046. S. Lorenzo in Campo. 32 pp.

Battistelli. A., Calore. C. and Pruess. K. (1993). A fluid property module for the TOUGH2 simulator for saline brines with non-condensible gas. *Proc 18th Workshop on* Geoth. *Res. Eng.*, Stanford University, Stanford, pp. 249-259.

McKibbin, R. and McNabb. A. (1993). Modelling the phase boundaries and fluid properties of the system H_2O-NaCl at high temperatures and pressures. *Proc. 15th NZ Geoth. Workshop.* Aukland, pp. 267-273.

O'Sullivan, M. J.. Bodvarsson. G. S.. Pruess. K. and Blakeley, M. R. (1985). Fluid and heat flow in gas-rich geothermal reservoirs. *SPE Jnl.*, pp. 215-226.

Pritchett, J. W.. Rice, M. H. and Riney T. D. (1981). *Equation-of-state for water-carbon dioxide mixtures. implications for Baca reservoir.* Report DOE/ET/27163-8, UC-66a. 53 pp.

Pritchett. J. W. (1993). *STAR User's Manual.* S-Cubed Report SSS-TR-89-10242. revision A.

Pruess. K. (1983). *Development of the general purpose simulator MULKOM.* Annual Report 1982, Earth Sciences Div., Lawrence Berkeley [Laboratory Report LBL-15500, Berkeley.

Pruess. K. and Narasimhan. T. N. (1985). A practical method for modeling fluid and heat flow in fractured porous media. *SPE Jnl.*, Vol. 25(1). pp. 11-16.

Pruess, K. (1991a). TOUGH2 - *A general-purpose numerical simulator for multi-phase fluid and heat flow.* Earth Sciences Div., Lawrence Berkeley laboratory Report LBL-29400, Berkeley. 102 pp

Pruess. K. (1991b). EOS7 - *An equation-of-state module for the TOUGH2 simulator for two-phase flow of saline water arid air.* Lawrence Berkeley Laboratory Report LBL-311 14. Berkeley. 17 pp.

Prueas. K. and O'Sullivan. M. (1992). Effects of capillarity and vapor adsorption in the depletion of vapor-dominated geothermal reservoirs. *Proc. 17th Workshop on Geoth. Res. Eng.*, Stanford University, Stanford, pp. 165-174.

Shook. G. M. (in press). Vapor pressure lowering in brines and implications for formation of a high temperature reservoir. *Proc. 19th Workshop on Geoth. Res. Eng.*, Stanford University. Stanford.

Thomas, G. W. (1982). *Principles of hydrocarbon reservoir simulation.* International Human Resources Development Corporation. Boston. p. 154.

Verma, A. and Pruess, K. (1988). Therniohydrological conditions and silica redistribution near high-level nuclear wastes emplaced in saturated geological formations. *Jnl. of Geophys. Res.*, Vol.93(B2), pp. 1159-1173.